Normal and torsional spring constants of atomic force microscope cantilevers

Christopher P. Green
Department of Mathematics and Statistics, University of Melbourne, Victoria 3010, Australia

Hadi Lioe
School of Chemistry, University of Melbourne, Victoria 3010, Australia

Jason P. Cleveland and Roger Proksch
Asylum Research, Santa Barbara, California 93117

Paul Mulvaney
School of Chemistry, University of Melbourne, Victoria 3010, Australia

John E. Sader[a)]
Department of Mathematics and Statistics, University of Melbourne, Victoria 3010, Australia

(Received 24 June 2003; accepted 8 March 2004; published online 21 May 2004)

Two methods commonly used to measure the normal spring constants of atomic force microscope cantilevers are the added mass method of Cleveland *et al.* [J. P. Cleveland *et al.*, Rev. Sci. Instrum. **64**, 403 (1993)], and the unloaded resonance technique of Sader *et al.* [J. E. Sader, J. W. M. Chon, and P. Mulvaney, Rev. Sci. Instrum. **70**, 3967 (1999)]. The added mass method involves measuring the change in resonant frequency of the fundamental mode of vibration upon the addition of known masses to the free end of the cantilever. In contrast, the unloaded resonance technique requires measurement of the unloaded resonant frequency and quality factor of the fundamental mode of vibration, as well as knowledge of the plan view dimensions of the cantilever and properties of the fluid. In many applications, such as frictional force microscopy, the torsional spring constant is often required. Consequently, in this article, we extend both of these techniques to allow simultaneous calibration of both the normal and torsional spring constants. We also investigate the validity and applicability of the unloaded resonance method when a mass is attached to the free end of the cantilever due to its importance in practice.
[DOI: 10.1063/1.1753100]

I. INTRODUCTION

Experimental determination of the spring constants of atomic force microscope (AFM) cantilevers is of fundamental importance in AFM applications. Currently, there exist many techniques capable of calibrating the normal spring constant.[1–5] However, in applications such as lateral force microscopy, knowledge of the torsional/lateral spring constant is of primary importance. Unfortunately, comparatively little research on calibration techniques for the torsional spring constant has appeared in the literature. Current methods typically require knowledge of the normal spring constant of the cantilever, which is then used to determine the torsional spring constant after a relationship between the two spring constants is established.[6–8] Alternatively, once the normal spring constant has been determined, theoretical formulas can be used to calculate the torsional spring constant.[4,9–11] This latter approach relies on knowledge of the Poisson ratio of the cantilever material, and is only valid for cantilevers composed of isotropic materials. For cantilevers made of crystalline materials, this approach can lead to inaccuracies, since the elastic properties of the cantilever can depend upon the mode of deformation.

In this article, we extend two commonly used normal spring constant calibration techniques to enable simultaneous determination of both the normal and torsional spring constants of AFM cantilevers.

(1) The added mass method of Cleveland *et al.*,[1] henceforth referred to as the *normal Cleveland method*, determines the normal spring constant by monitoring the change in the fundamental resonant frequency of flexural vibration upon addition of known masses to the free end of the cantilever. An important feature of this calibration method is that it is valid for any cantilever, regardless of the geometry or material properties, making it universally applicable. However, the requirement for the addition of masses makes this technique destructive.
(2) The unloaded resonance method of Sader *et al.*,[2] henceforth referred to as the *normal Sader method*, is principally concerned with the normal spring constant of rectangular AFM cantilevers. It requires measurement of the resonant frequency and quality factor of the fundamental flexural mode in fluid (typically air), as well as knowledge of the plan view dimensions of the cantilever. As

[a)]Author to whom correspondence should be addressed; electronic mail: jsader@unimelb.edu.au

such, this method is nondestructive, noninvasive, and allows rapid determination of the normal spring constant of rectangular cantilevers. It can also be extended to other cantilever geometries, as discussed in Ref. 2.

Extensions of the aforementioned calibration techniques to measurement of the torsional spring constant shall henceforth be referred to as the *torsional Cleveland method* and *the torsional Sader method*, respectively. Derivation of the torsional Cleveland method will draw on classical torsion theory, while the torsional Sader method utilizes results of a recent theoretical study of the torsional frequency response of cantilever beams immersed in viscous fluids.[12] Since each of these torsional extensions involves an experimental setup identical to its normal counterpart, no additional effort is required to obtain the torsional spring constant. Consequently, simultaneous calibration of both the normal and torsional spring constant is possible using these techniques.

We commence by briefly reviewing the normal Cleveland method and then formulating its extension to the torsional spring constant. A brief review of the normal Sader method is then presented, followed by its extension to the torsional spring constant. Important features of both extensions are discussed. These techniques are then validated experimentally, and results compared. Finally, we investigate the effect of an attached mass on the accuracy of both the normal and torsional Sader methods due to its relevance to AFM applications, such as colloid probe measurements.

II. THEORY

The spring constant of a cantilever relates the load applied to subsequent deformation of the cantilever. Specifically, the normal spring constant k_z connects the flexural deflection Δz due to an applied normal force N,

$$k_z = \frac{N}{\Delta z}, \tag{1}$$

whereas the torsional spring constant k_ϕ relates the torsional deflection $\Delta\phi$ to an applied torque T,

$$k_\phi = \frac{T}{\Delta\phi}. \tag{2}$$

For a schematic illustration of these two types of deformation; see Figs. 1(a) and 1(b), respectively.

In the following derivations, we use a subscript (or superscript) f or t to refer to flexural or torsional vibrations, respectively.

A. Cleveland methods

1. Normal Cleveland method

The normal Cleveland method involves monitoring the change in fundamental flexural resonant frequency due to the addition of known masses to the free end of the cantilever. These applied masses are typically spherical. The relationship between the added mass M_s and the fundamental radial resonant frequency of flexural vibration ω_f is

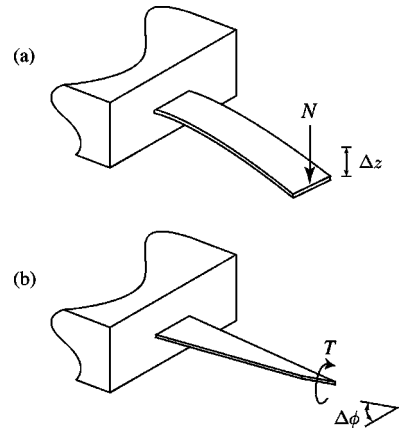

FIG. 1. Schematic illustration of (a) the flexural deflection Δz of a cantilever due to applied normal force N and (b) the torsional deflection $\Delta\phi$ of a cantilever due to applied torque T.

$$M_s = \frac{k_z}{\omega_f^2} - m_e, \tag{3}$$

where k_z is the normal spring constant and m_e is the effective mass of the cantilever. Attaching several different masses and measuring the corresponding resonant frequency enables the normal spring constant k_z to be determined from the slope of a linear plot of M_s vs ω_f^{-2}.

2. Torsional Cleveland method

We now extend the Cleveland method to enable calibration of the torsional spring constant. The fundamental radial resonant frequency of torsional vibration ω_t of a cantilever of arbitrary geometry is given by

$$\omega_t^2 = \frac{k_\phi}{J_e}, \tag{4}$$

where k_ϕ is the torsional spring constant of the cantilever, and J_e its effective mass moment of inertia. With the addition of a mass (with mass moment of inertia J) to the free end of the cantilever, the radial resonant frequency of torsional vibration becomes[13,14]

$$\omega_t^2 = \frac{k_\phi}{J + J_e}. \tag{5}$$

For a spherical added mass of radius r and mass M_s, the mass moment of inertia J_s about its axis is given by[13]

$$J_s = \tfrac{2}{5} M_s r^2. \tag{6}$$

Assuming that the sphere is placed at the free end of the cantilever with its center aligned on the major axis of the cantilever, and provided the diameter of the sphere is much greater than the thickness of the cantilever,[15] the total added mass moment of inertia due to the sphere J_s can be calculated using the parallel axis theorem,[13]

$$J_s = \tfrac{7}{5} M_s r^2. \tag{7}$$

Substituting Eq. (7) in Eq. (5), we obtain

$$\omega_t^2 = \frac{k_\phi}{7/5 M_s r^2 + J_e}. \tag{8}$$

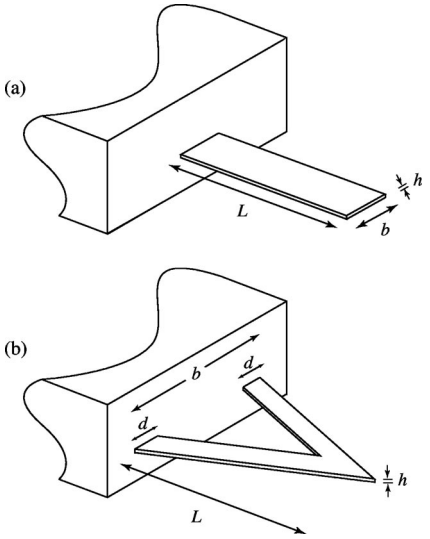

FIG. 2. Schematic illustration of the plan view dimensions of (a) a rectangular cantilever and (b) a V-shaped cantilever.

Rearranging Eq. (8) and expressing the mass in terms of the radius r and density ρ_s of the sphere, we obtain

$$\frac{28\pi\rho_s r^5}{15} = \frac{k_\phi}{\omega_t^2} - J_e . \tag{9}$$

Clearly, if several different spheres are attached with their centers aligned on the major axis of the cantilever at its free end, then a plot of $J_s = 28\pi\rho_s r^5/15$ vs ω_t^{-2} will be linear, with a gradient equal to the torsional spring constant k_ϕ. Furthermore, the effective mass moment of inertia of the cantilever is given by the negative intercept with the vertical axis.

3. Off-end loading

The theory presented above assumes that the spherical masses are placed at an identical position on the cantilever. Consequently, this would yield the spring constants at that position. In practice, however, the spring constant may be required away from this position. For the case of a rectangular cantilever beam of length L, it is known that normal spring constant k_z, evaluated when the load is applied a distance ΔL from the free end, is related to the normal spring constant at the end of the cantilever, k_z^E, by[16]

$$k_z = k_z^E \left(\frac{L}{L-\Delta L} \right)^3 . \tag{10}$$

This equation holds for both rectangular and V-shaped cantilevers,[16,17] schematics of which are given in Fig. 2.

The situation is very different, however, for the torsional spring constant. Using beam theory, it is simple to show that torsional spring constant k_ϕ of a rectangular cantilever at distance ΔL from its free end is related to the spring constant at the end k_ϕ^E, by

$$k_\phi = k_\phi^E \left(\frac{L}{L-\Delta L} \right). \tag{11}$$

Note that the dependence upon the lengthwise positioning of the load is much stronger for the normal spring constant than it is for the torsional spring constant; cf. Eqs. (10) and (11).

For cantilevers of other geometries, the situation can be more complex. One such example is the commonly used V-shaped cantilever, where the torsional spring constant is extremely sensitive to lengthwise positioning of the load.[18] Indeed, it is absolutely necessary to apply the load away from the end of the cantilever if it comes to a point, because the V-shape geometry is unable to support a torque applied at its very end-tip, where its torsional rigidity is zero.[19] This is an important consideration when trying to determine the torsional spring constant of V-shaped AFM cantilevers. This undesirable property can significantly complicate calibration and application of V-shaped cantilevers in torsional/lateral force measurements.

4. Off-axis loading

All of the above theoretical formulas implicitly assume that the load is applied on the major axis of the cantilever. We now consider the effect of lateral displacement of the spherical mass away from the major axis of the cantilever, which we term *off-axis loading*.

It has been shown using finite-element analysis that deviation in the normal spring constant due to off-axis loading is small for both rectangular and V-shaped cantilevers.[16] A similar approach shows that the effect of off-axis loading on the torsional spring constant also results in only small deviations from the on-axis values for both rectangular and V-shaped cantilevers, provided that the load is applied on the neutral axis of the cantilever.[20] For example, the torsional spring constant of a rectangular cantilever of aspect ratio $L/b = 10$ [see Fig. 2(a)], varies by at most 2% when the load is applied off-axis. Similar results are observed for V-shaped cantilevers.

Experimentally, the off-axis application of a spherical mass in the normal Cleveland method has been demonstrated to have very little effect on the measured resonant frequency, and consequently the measured normal spring constant.[16] However, off-axis application of a spherical mass introduces some experimental difficulties for the torsional Cleveland method. If the spherical mass is applied away from the major axis of the cantilever, the total mass moment of inertia due to the sphere becomes

$$J_s = \left[\frac{7}{5} + \left(\frac{e}{r} \right)^2 \right] M_s r^2, \tag{12}$$

where e is the projected distance between the center of mass of the sphere and the axis of rotation onto the plane of the cantilever. It then follows that the mass moment of inertia of a sphere applied off axis is larger than that of an identical sphere applied on the major axis of the cantilever, cf. Eqs. (7) and (12). This increase in mass moment of inertia will cause the frequency of torsional vibration to decrease; see Eq. (5). However, any off-axis positioning of the spherical mass leads to coupling of the flexural and torsional modes of vibration.[21] This greatly complicates the resulting analysis. Hence, we do not derive an explicit theoretical result for this

case, but instead experimentally examine the effect of off-axis application of the spherical masses on the measured torsional spring constant in Sec. III.

B. Sader methods

1. Normal Sader method

The normal Sader method for calibrating the normal spring constant of rectangular AFM cantilevers involves measurement of the unloaded radial resonant frequency ω_f and quality factor Q_f of the fundamental flexural resonance peak for a cantilever beam immersed in fluid, typically air. Provided the quality factor is much greater than unity, which is typically satisfied if the cantilever is immersed in air, the normal spring constant at the end-tip of the cantilever is given by[2]

$$k_z = 0.1906 \rho b^2 L Q_f \omega_f^2 \Gamma_i^f(\omega_f), \tag{13}$$

where ρ is the density of the fluid, b and L are the width and length of the cantilever, respectively, and Γ_i^f is the imaginary component of the hydrodynamic function given by Eq. (20) of Ref. 22.

2. Torsional Sader method

We now extend the normal Sader method to the related problem of calibrating the torsional spring constant of a rectangular cantilever beam, which is derived in an an analogous manner to the normal Sader method. Assuming the length L of the cantilever beam is much greater than its width b, which in turn greatly exceeds its thickness h, it can be easily shown that the torsional spring constant k_ϕ at its end-tip is given by[23]

$$k_\phi = \frac{1}{3\pi^2} \rho_c b^3 h L \omega_{t,\mathrm{vac}}^2, \tag{14}$$

where ρ_c is the density of the cantilever, and $\omega_{t,\mathrm{vac}}$ is the fundamental radial resonant frequency of torsional vibration in vacuum.

Equation (14) is of limited use, however, due to the difficulty in measuring both the cantilever mass ($\rho_c bhL$) and resonant frequency in vacuum. Consequently, we refer to the recent theoretical model for the torsional frequency response of cantilever beams immersed in viscous fluids by Green and Sader.[12] Provided the quality factor of the torsional resonance peak is much greater than unity, it follows that the vacuum radial resonant frequency of torsional vibration $\omega_{t,\mathrm{vac}}$ can be directly related to the radial resonant frequency of torsional vibration in fluid ω_t, by

$$\omega_{t,\mathrm{vac}} = \omega_t \left(1 + \frac{3\pi\rho b}{2\rho_c h} \Gamma_r^t(\omega_t) \right)^{1/2}, \tag{15}$$

where ρ is the density of the fluid, and Γ_r^t is the real part of the (known) hydrodynamic function $\Gamma^t(\omega)$; see Fig. 3. An analytic expression for $\Gamma^t(\omega)$ is given in Eq. (20) of Ref. 12. Importantly, $\Gamma^t(\omega)$ depends only upon the Reynolds number $\mathrm{Re} = \rho\omega b^2/(4\eta)$, where η is the fluid viscosity and ω is the radial torsional frequency, and is independent of the cantilever thickness and density.

In addition, the areal mass density $\rho_c h$ is given by[12]

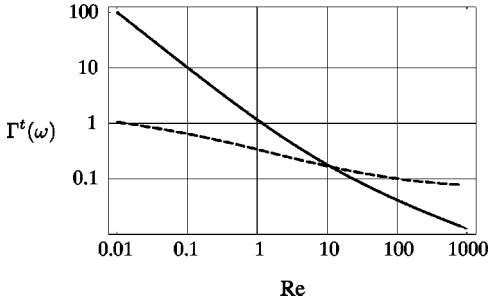

FIG. 3. Hydrodynamic function $\Gamma^t(\omega)$ for a rectangular cantilever beam as a function of the Reynolds number $\mathrm{Re} = \rho\omega b^2/(4\eta)$. The dashed line is the real component $\Gamma_r^t(\omega)$, while the solid line is the imaginary component $\Gamma_i^t(\omega)$.

$$\rho_c h = \frac{3\pi\rho b}{2} [Q_t \Gamma_i^t(\omega_t) - \Gamma_r^t(\omega_t)], \tag{16}$$

where Q_t is the quality factor of the fundamental torsional resonance peak, and $\Gamma_i^t(\omega)$ is the imaginary part of the hydrodynamic function $\Gamma^t(\omega)$. Substituting Eqs. (15) and (16) in Eq. (14), we then obtain

$$k_\phi = 0.1592 \rho b^4 L Q_t \omega_t^2 \Gamma_i^t(\omega_t). \tag{17}$$

Equation (17) is the required result, and it relates the torsional spring constant at the end tip of the cantilever k_ϕ to its plan view dimensions L and b, and the resonant frequency ω_t and quality factor Q_t of the fundamental resonance peak of torsional vibration in fluid. It is important to emphasize that this expression is valid provided $Q_t \gg 1$, which is typically satisfied in practice, especially for a cantilever immersed in air. Furthermore, the inherent assumption that the length of the cantilever greatly exceeds its width, which in turn greatly exceeds its thickness, is also typically satisfied.

3. Non-rectangular cantilevers

The normal and torsional spring constants of cantilevers with non-rectangular geometries can be calibrated indirectly using the Sader methods, as we shall now discuss. To begin, we note that the material properties and thickness of all cantilevers on a single chip are typically identical. Consequently, provided the chip under consideration has multiple cantilevers attached, and at least one of these cantilevers is rectangular in geometry, then the spring constants of the non-rectangular cantilevers can be easily determined as follows.

As discussed in Ref. 2, the normal spring constant of the rectangular cantilever is first measured, from which the rigidity Eh^3, where E is the Young's modulus of the cantilever, is then evaluated,

$$Eh^3 = k_z \frac{4L^3}{b}. \tag{18}$$

Using this known rigidity and the plan view dimensions of the cantilever in question, theoretical results for the normal spring constants of the non-rectangular cantilevers can then be used to determine their normal spring constants.[11,18,24]

The torsional spring constant of non-rectangular cantilevers can be found in an analogous manner. Namely, the torsional spring constant of the rectangular cantilever is first

TABLE I. Summary of formulas for the Cleveland and Sader methods for normal spring constant k_z and torsional spring constant k_ϕ, derived in Sec. II.

Method	Formula
Normal Cleveland	$M_s=\frac{k_z}{\omega_f^2}-m_e$
Torsional Cleveland	$\frac{28\pi\rho_s r^5}{15}=\frac{k_\phi}{\omega_t^2}-J_e$
Normal Sader	$k_z=0.1906\rho b^2 L Q_f \omega_f^2 \Gamma_i^f(\omega_f)$
Torsional Sader	$k_\phi=0.1592\rho b^4 L Q_t \omega_t^2 \Gamma_i^t(\omega_t)$

measured, from which the torsional rigidity Gh^3, where G is the shear modulus of the cantilever, is evaluated using the result

$$Gh^3=k_\phi\frac{3L}{b}. \tag{19}$$

Theoretical results for the torsional spring constants of nonrectangular cantilevers[11,18,24] can then be used to calibrate these cantilevers, since these results rely on the torsional rigidity and plan view dimensions.

Importantly, neither of these methods requires any knowledge of the elastic properties of the cantilever, quantities that are difficult to measure in practice.

Finally, a summary of the principal formulas derived in Sec. II is presented in Table I.

III. EXPERIMENTAL RESULTS

We now assess the validity of the calibration techniques derived above by presenting a detailed experimental comparison. Three types of cantilevers are used in this assessment, all of which were procured from Veeco.[25] Details of the geometries and plan view dimensions of all cantilevers are given in Table II.

The first set consist of one rectangular cantilever and several V-shaped cantilevers on a single chip. These cantilevers have imaging tips and are composed of uncoated Si_3N_4. Measurements were performed on the rectangular cantilever, R_1, and two V-shaped cantilevers, denoted V_1 and V_2.

The second set of cantilevers are micromachined from single crystal silicon, and consequently have accurately specified dimensions and material properties.[26] Only the longest rectangular cantilever, denoted R_2, was used, since it has a torsional resonant frequency below 500 kHz, which is the highest frequency attainable using our instrumentation.

TABLE II. Cantilever dimensions. Rectangular cantilevers: R_1 (Si_3N_4), R_2 (single crystal silicon), and R_3 (gold coated Si_3N_4). V-shaped cantilevers: V_1 and V_2 (both Si_3N_4), and V_3 (gold coated Si_3N_4). Geometric parameters are shown in Fig. 2. All measurements were performed using an optical microscope.

Cantilever	L (μm)	b (μm)	d (μm)
R_1	197	19	⋯
R_2	422	29	⋯
R_3	205	19.5	⋯
V_1	323	215	21
V_2	219	150	21
V_3	317	222	22

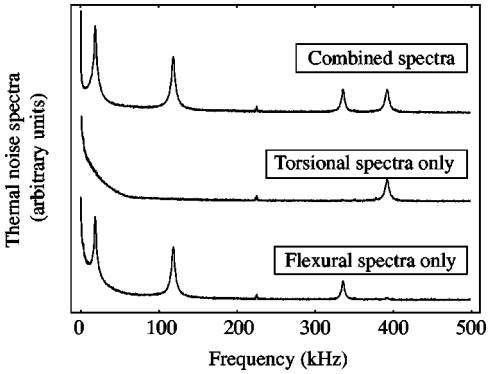

FIG. 4. Thermal noise spectra due to flexural vibration only (bottom), torsional vibration only (middle) and combined spectra (top). The vertical offset is arbitrary and for illustrative purposes only. All plots have identical logarithmic vertical scales.

The third set of cantilevers consist of gold coated Si_3N_4 rectangular and V-shaped cantilevers on a single chip. The rectangular cantilever, denoted R_3, and the V-shaped cantilever adjacent to it, V_3, were used in experiments to verify that the calibration techniques are also applicable to cantilevers made of composite materials.

Both experimental techniques rely on measurement of the cantilever resonant frequency. For the normal spring constant, the flexural resonant frequency is required, while for the torsional spring constant, the torsional resonant frequency must be measured. Using a split quadrant photodiode detector, which is common in many commercial AFMs, it is possible to collect the flexural and torsional frequency responses individually or collectively, as demonstrated in Fig. 4. By selecting the appropriate signals from the detector, it is easy to distinguish between flexural and torsional resonance peaks. In addition, combined measurement of the flexural and torsional signals enables simultaneous calibration of the normal and torsional spring constants using either technique described above, provided it is known which peaks correspond to the flexural and torsional resonances.

All measurements were conducted in air, satisfying the fundamental requirement of both Sader methods that the quality factors greatly exceed unity. To measure the resonant frequency ω (required for the Cleveland and Sader methods), and the corresponding quality factor Q (required for the Sader methods only), the thermal noise spectra of the cantilevers were measured.[27] The resonant frequency and quality factor of the resonance peak were then obtained by fitting this signal with the response of a simple harmonic oscillator. To ensure accurate fits, a white noise floor was included in the fitting procedure.[2,30] This approach enabled accurate determination of the resonant frequency and quality factors to within $\pm 0.1\%$ and $\pm 1\%$, respectively.

In all cases, the thermal noise spectra were sufficiently strong that no active excitation of the cantilevers was required. Nonetheless, to examine the applicability of such excitation, we also drove the R_1 cantilever by vibrating its base using tapping mode cantilever tuning software.[31] This induced normal oscillations at the base of the cantilever. In all

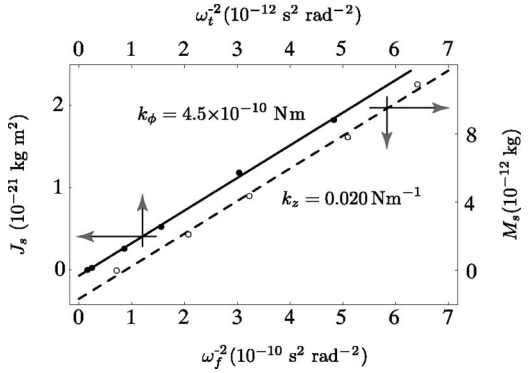

FIG. 5. Application of Cleveland methods: Torsional (solid line and closed circles) and normal (dashed line and open circles) for the R_1 cantilever. Straight lines are fits to experimental data (circles), the slopes of which give the spring constants. Density of tungsten spheres: $\rho_{\mathrm{tung}} = 19\,250\ \mathrm{kg\,m^{-3}}$.

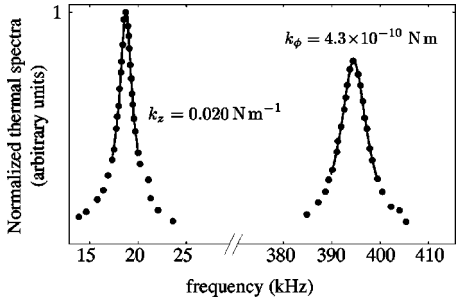

FIG. 6. Application of the Sader methods. Measured thermal noise spectrum (closed circles) fitted with the response of the simple harmonic oscillator (Ref. 30) (solid lines) for the R_1 cantilever. For clarity, some data points were removed.

cases, we were able to extract the flexural and torsional resonance peaks using this approach. These measurements agreed to a high degree of accuracy with those of the thermal noise spectra for both the resonant frequencies and quality factors. This behavior is expected, provided the drive amplitudes are not large enough to introduce nonlinearities.

It is interesting that both normal and torsional vibrations are induced by purely normal excitation at the base of the cantilever. A possible reason for this is that the plane of the cantilever is not perfectly level with the horizontal.

A. Comparison of Cleveland and Sader methods

The applicability of the Cleveland and Sader methods to simultaneous measurement of both the normal and torsional spring constants is now assessed. For the Cleveland methods, tungsten spheres of differing diameters were attached to the free end of the cantilever, with their centers lying on the major axis of the cantilever.[32] A small amount of petroleum jelly was used to attach the tungsten spheres to the cantilevers to allow more accurate reproducible placement. The addition of petroleum jelly has a negligible effect on measured resonant frequencies, because its mass is much smaller than that of the tungsten spheres. No discernible shift in resonant frequency was observed when the jelly was applied to the cantilever. The thermal noise spectrum was then measured for each attached sphere, from which both the flexural and torsional resonant frequencies were simultaneously determined. The diameters of the spheres were measured using an optical microscope (to within accuracy of $\pm 1\%$), from which the mass M_s and mass moment of inertia J_s of the applied spheres were then calculated. Figure 5 shows plots of the added mass and added mass moment of inertia as functions of ω_f^{-2} and ω_t^{-2}, respectively, for rectangular cantilever R_1. It is strikingly evident that both plots are linear. This agrees with the theoretical formalism presented in Sec. II, and allows immediate simultaneous determination of the normal and torsional spring constants. Analogous results for the Sader methods are presented in Fig. 6. In contrast to the Cleveland methods, all that is required in this case is a single measurement of the thermal noise spectrum, from which both k_z and k_ϕ are determined.

In Table III, we present a detailed comparison of these techniques for the three rectangular cantilevers, R_1, R_2 and R_3. It is clear that good agreement between the Sader and Cleveland methods is obtained for both the normal and torsional spring constants for all cases. We emphasize that, in both methods, the torsional and normal spring constants are obtained simultaneously and independently of each other. These results demonstrate the validity of these different yet complementary techniques for the case of rectangular cantilevers.

In Table III, we also compare the torsional spring constant k_ϕ^{calc} obtained by first measuring the normal spring constant k_z, and then applying the following theoretical result (for rectangular cantilevers):[11]

$$k_\phi = k_z \frac{2L^2}{3(1+\nu)}, \tag{20}$$

where ν is the Poisson ratio of the cantilever. This approach was proposed in Ref. 9. In the absence of a measurement of the Poisson ratio, a nominal value of $\nu = 0.25$ was used for all cases. In this study, k_z was obtained using the normal Cleveland method, although any method for measuring the normal spring constant can be used. Note that Eq. (20) is strictly valid for cantilevers composed of isotropic materials only, whose aspect ratios L/b are large. For the R_1 and R_3 cantilevers, which are composed of isotropic materials, the torsional spring constants obtained in this manner agree well with those obtained using the torsional Cleveland and torsional Sader methods, with errors $<10\%$. This is expected, since the Poisson ratio of Si_3N_4 is known to lie between 0.2 and 0.3.[6,33,34] Thus, the choice of $\nu = 0.25$ results in only 5% uncertainty. The resulting comparison therefore confirms the validity of both the torsional Cleveland and torsional Sader methods. For the R_2 cantilever, however, the result obtained using Eq. (20) differs significantly, with a discrepancy of more than 20%. This error is due to the R_2 cantilever being composed of a crystalline material, whose elastic properties depend upon the mode of deformation, whereas Eq. (20) is derived for an isotropic material.

Results obtained using the Cleveland and Sader methods for the three V-shaped cantilevers are presented in Table IV. Again, note the good agreement between these methods, for both the normal and torsional spring constants. The Cleveland methods are implemented in exactly the same manner as for the rectangular cantilevers. It is important to note that

TABLE III. Rectangular cantilevers. Comparison of spring constants determined by the Sader methods (superscript Sader); Cleveland methods (superscript Clev); and Eq. (20) (superscript calc). f and Q are the resonant frequency and quality factor, respectively. Subscripts f and t refer to flexural and torsional cases, respectively. Measurements were performed in air: $\rho = 1.18\ \mathrm{kg\,m^{-3}}$ and $\eta = 1.86\times10^{-5}\ \mathrm{kg\,m^{-1}\,s^{-1}}$.

Cantilever	f_f (kHz)	Q_f	f_t (kHz)	Q_t	k_z^{Sader} ($\mathrm{N\,m^{-1}}$)	k_ϕ^{Sader} (10^{-10} N m)	k_z^{Clev} ($\mathrm{N\,m^{-1}}$)	k_ϕ^{Clev} (10^{-10} N m)	k_ϕ^{calc} (10^{-10} N m)
R_1	18.78	17.2	393.4	104	0.020	4.3	0.020	4.5	4.1
R_2	10.12	25.4	258.3	167	0.037	26	0.037	28	35
R_3	15.39	20.9	314.5	123	0.020	4.2	0.020	4.1	4.5

care must be taken in positioning the spherical masses when calibrating the torsional spring constants of V-shaped cantilevers. This is because the strong dependence of the torsional spring constant of V-shaped cantilevers on lengthwise positioning of the load[18] necessitates that each sphere be placed in the same position to a high degree of accuracy. This introduces some experimental difficulties into the calibration procedure. Furthermore, as discussed previously, the spheres must be attached away from the end of the cantilever if it comes to a point; see Fig. 2(b). The V-shaped cantilevers used in this study, V_1, V_2, and V_3, however, all had their end-tips trimmed so that they did not meet at a point. Consequently, the spheres could be applied at the end in this case. We note that the spring constants measured using the Cleveland methods correspond to those at distance ΔL from the center of the attached sphere to the projected end-tip point.

The Sader methods were also used to calibrate both the normal and torsional spring constants of the V-shaped cantilevers. This was possible because all three V-shaped cantilevers have a rectangular cantilever present on the same chip. Using the methodology presented in Sec. II, k_z and k_ϕ for the rectangular cantilever were first measured using the Sader methods. The normal and torsional spring constants of the V-shaped cantilever were then obtained from the measured plan view dimensions of both cantilevers, using the appropriate theoretical formulas.[17–19] We stress that this approach is only valid when a rectangular cantilever is present on the same chip as the V-shaped cantilever in question.

These results, combined with those for the rectangular cantilevers above, therefore demonstrate the applicability of the Cleveland and Sader methods in simultaneous measurement of both the normal and torsional spring constants.

B. Torsional Cleveland method: Off-axis loading

We now investigate the applicability of the torsional Cleveland method for cases where the added masses are attached away from the major axis of the cantilever. Results obtained by applying the spheres as close as possible to the side edge of the R_1 cantilever are presented in Fig. 7, along with results for spheres attached along the major axis of the cantilever. Applying Eq. (9), which is derived for attachment on the major axis, leads to a measured torsional spring constant approximately 25% smaller than the corresponding on-axis value. This behavior is due to the increase in mass moment of inertia J_s of the sphere with off-axis loading and coupling of the flexural and torsional modes, which is not taken into account in Sec. II due to its complexity. Nonetheless, since the spheres are attached at the maximum distance from the major axis ($\sim 9\ \mu$m away), these results represent the worst case scenario. As such, the error in measured torsional spring constant due to off-axis application of the spheres will be smaller for cases where the spheres are positioned closer to the major axis of the cantilever, as demonstrated above. In contrast to this finding, we remind the reader that the normal Cleveland method is insensitive to off-axis loading of the spheres.[16]

TABLE IV. V-shaped cantilevers. Comparison of spring constants determined by the Cleveland methods (superscript Clev); and the Sader methods (superscript Sader). Spring constants evaluated a distance ΔL from the end tip projected to a point. The Sader methods were implemented by first calibrating a rectangular cantilever and then applying the formulas in Refs. 18, 17, and 19.

Cantilever	ΔL (μm)	k_z^{Clev} ($\mathrm{N\,m^{-1}}$)	k_ϕ^{Clev} (10^{-10} N m)	k_z^{Sader} ($\mathrm{N\,m^{-1}}$)	k_ϕ^{Sader} (10^{-10} N m)
V_1	35	0.013	6.8	0.013	6.6
V_2	20	0.037	8.7	0.038	8.7
V_3	31	0.014	6.4	0.014	6.1

C. Sader methods: Effect of added mass

In practice, many AFM measurements are performed with a colloidal probe attached to the free end of the cantilever. Consequently, here in Sec. III C we investigate the effect of such added mass on the accuracy and validity of the Sader methods. Rectangular cantilevers only are considered, since the Sader methods are primarily applicable to these cantilevers. Results of this investigation using the R_1 cantilever for both the normal and torsional Sader methods are presented in Tables V and VI, respectively.

To begin, we consider the normal Sader method. Application of a mass to the free end of the cantilever, while not affecting its normal spring constant, will result in a decrease

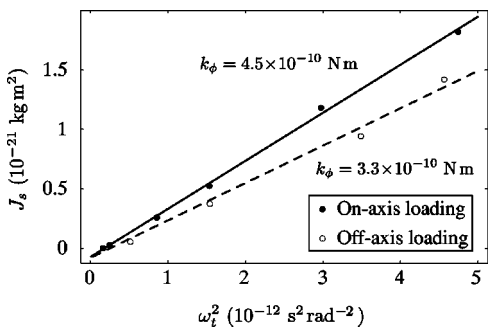

FIG. 7. Effect of off-axis loading on measured k_ϕ of the R_1 cantilever using the torsional Cleveland method. On-axis loading (closed circles); off-axis loading (open circles). The off-axis distance $\sim 9\ \mu$m.

TABLE V. Effect of added mass on the normal Sader method for the R_1 cantilever for tungsten and silica spheres. D is the diameter of the sphere, f_f and Q_f are the resonant frequency and quality factor, respectively, of the fundamental flexural resonance, M_s is the mass of the spheres, and m_c is the mass of the cantilever [measured using the plan view dimensions and Eq. (3) in Ref. 2]. Density of tungsten $\rho_{\text{tung}}=19\,250\ \text{kg m}^{-3}$ density of silica $\rho_{\text{silica}}=2400\ \text{kg m}^{-3}$. All measurements were performed in air.

Sphere	D (μm)	f_f (kHz)	Q_f	M_s/m_c	k_z (N m^{-1})
Tungsten	0	18.10	17.1	0	0.020
	7	11.23	29.7	0.48	0.019
	8	8.91	40.2	0.93	0.018
	9	7.93	45.0	1.36	0.018
	10	6.82	47.8	1.90	0.016
Silica	7	16.29	19.2	0.08	0.020
	8	15.61	19.8	0.12	0.019
	9	13.96	23.0	0.17	0.019
	12	12.31	25.2	0.37	0.017
	14	11.16	27.4	0.54	0.017

in resonant frequency ω_f and an increase in quality factor Q_f. A decrease in ω_f, however, leads to an increase in the imaginary component of the hydrodynamic function $\Gamma_i^f(\omega_f)$; see Fig. 1 of Ref. 2. These increases in Q_f and $\Gamma_i^f(\omega_f)$ do not quite balance the decrease in ω_f^2 in Eq. (13). Consequently, the measured normal spring constant is smaller when a mass is attached to the free end of the cantilever than the result obtained for an unloaded cantilever (the actual value). This is evident in Table V, where it is clear that, as the diameter of the spheres increases, the normal spring constant measured using the normal Sader method decreases. These results indicate that the size of the sphere, and not its mass, is primarily responsible for the decrease in measured normal spring constant. For example, tungsten and silica spheres of the same size result in a similar decrease in measured normal spring constant, although the heavier tungsten spheres slightly enhance this decrease. These results suggest that the contributing error in the normal Sader method is less than 10% for a cantilever with an attached spherical mass, provided the sphere diameter is less than approximately half the width of the cantilever.

Next, we consider the effect of an attached spherical mass on the accuracy of the torsional Sader method. As demonstrated in Table VI, the torsional spring constant obtained with a silica sphere attached to the major axis of the cantilever at its free end differs significantly from the value obtained for the unloaded cantilever. As the sphere gets larger, this difference increases. Similar results are obtained for tungsten masses. While the resonant frequency of torsional vibration decreases as the diameter of the sphere increases, the quality factor is seen to have no particular trend, which is nonsensical. This is most likely due to the nonrigid bond between the sphere and the cantilever, which is probed by the twisting motion of the cantilever. This undesirable property is not present in the normal Sader method, since flexural deflection of the cantilever does not probe this nonrigid bond.

TABLE VI. Effect of added mass on the torsional Sader method for the R_1 cantilever for silica spheres. D is the diameter of the sphere, f_t and Q_t are the resonant frequency and quality factor, respectively, of the fundamental torsional resonance, J_s is the mass moment of inertia of the spheres, and J_c is the mass moment of inertia of the cantilever (determined using $J_c=m_c b^2/12$) (Ref. 13). The mass of the cantilever m_c is measured using the plan view dimensions and Eq. (16). Density of silica $\rho_{\text{silica}}=2400\ \text{kg m}^{-3}$. All measurements were performed in air.

D (μm)	f_t (kHz)	Q_t	J_s/J_c	k_ϕ (10^{-10} N m)
0	393.4	103	0	4.3
7	382.4	96.2	0.04	3.8
8	372.2	103	0.09	4.0
9	338.1	100	0.17	3.4
14	236.1	74.7	1.16	1.6

These results indicate that the normal Sader method is capable of providing an accurate measurement when a sphere is attached to the free end of the cantilever. However, this is not true for the torsional Sader method, in which spurious measurements can result.

We have presented extensions of both the normal Cleveland and normal Sader methods to enable calibration of the torsional spring constants of AFM cantilevers. These extensions, referred to as the torsional Cleveland and torsional Sader methods, respectively, allow direct experimental determination of the torsional spring constants of AFM cantilevers, and show good agreement for both rectangular and V-shaped cantilevers. Since these torsional extensions utilize an experimental setup identical to that of their normal spring constant counterparts, they enable direct and simultaneous calibration of both normal and torsional spring constants of AFM cantilevers.

In order to assist in implementation of the Sader and torsional Sader methods, the authors have made available an online calibration program, located at http://www.ampc.ms.unimelb.edu.au/afm. Also available at that address are Mathematica files which calculate the spring constants using the aforementioned techniques.

ACKNOWLEDGMENTS

This research was supported by the Particulate Fluids Processing Center of the Australian Research Council and the Australian Research Council Grants Scheme. One of the authors (C.P.G.) gratefully acknowledges support of an Australian Postgraduate Award.

[1] J. P. Cleveland, S. Manne, D. Bocek, and P. K. Hansma, Rev. Sci. Instrum. **64**, 403 (1993).
[2] J. E. Sader, J. W. M. Chon, and P. Mulvaney, Rev. Sci. Instrum. **70**, 3967 (1999).
[3] J. L. Hutter and J. Bechhoefor, Rev. Sci. Instrum. **64**, 1868 (1993).
[4] C. T. Gibson, G. S. Watson, and S. Myhra, Nanotechnology **7**, 259 (1996).
[5] T. J. Senden and W. A. Ducker, Langmuir **10**, 1003 (1994).
[6] D. F. Ogletree, R. W. Carpick, and M. Salmeron, Rev. Sci. Instrum. **67**, 3298 (1996).
[7] G. Bogdanovic, A. Meurk, and M. W. Rutland, Colloids Surf., B **19**, 397 (2000).
[8] A. Feiler, P. Attard, and I. Larson, Rev. Sci. Instrum. **71**, 2746 (2000).
[9] R. G. Cain, S. Biggs, and N. W. Page, J. Colloid Interface Sci. **227**, 55 (2000).
[10] E. Liu, B. Blanpain, and J. P. Celis, Wear **192**, 141 (1996).
[11] W. C. Young, *Roark's Formulas for Stress and Strain*, 6th ed. (McGraw–Hill, New York, 1989).
[12] C. P. Green and J. E. Sader, J. Appl. Phys. **92**, 6262 (2002).

[13] K. Gieck and R. Gieck, *Engineering Formulas* (McGraw–Hill, New York, 1997).
[14] Using finite element analysis, (Ref. 20) it is found that the distance between the center of the mass and the neutral axis of the cantilever, when the mass is aligned with the major axis of the cantilever, has an insignificant effect on the torsional mode of deformation, i.e., coupling into other modes is negligible.
[15] This condition is typically satisfied in practice.
[16] J. E. Sader, I. Larson, P. Mulvaney, and L. R. White, Rev. Sci. Instrum. **66**, 3789 (1995).
[17] J. E. Sader, Rev. Sci. Instrum. **66**, 4583 (1995).
[18] J. M. Neumeister and W. A. Ducker, Rev. Sci. Instrum. **65**, 2527 (1994).
[19] J. E. Sader, Rev. Sci. Instrum. **74**, 2438 (2003).
[20] LUSAS, Finite Element Analysis Ltd., Forge House, 66 High St., Kingston upon Thames, Surrey KT1 1HN, UK.
[21] S. Timoshenko, D. H. Young, and W. Weaver, *Vibration Problems in Engineering* (Wiley, New York, 1974).
[22] J. E. Sader, J. Appl. Phys. **84**, 64 (1998).
[23] A. E. H. Love, *A Treatise on the Mathematical Theory of Elasticity* (Pergamon, London, 1959).
[24] J. E. Sader, in *Encyclopedia of Surface and Colloid Science*, edited by A. Hubbard (Dekker, New York, 2002), pp. 846–856.
[25] Veeco, 1171 Borregas Ave., Sunnyvale, CA 94089.
[26] M. Tortonese and M. Kirk, Proc. SPIE **3009**, 53 (1997).
[27] The signal was collected and digitized using a data acquisition board (Ref. 28). Multiple measurements were taken. These were then windowed together using a Hanning function, fast Fourier transformed, and finally averaged together to obtain the required thermal noise spectra (Ref. 29).
[28] National Instruments, 6504 Bridge Point Parkway, Austin, TX 78730-5039. The model used was the AT-MIO-16E-1 DAQ.
[29] LabVIEW software, available from National Instruments (see Ref. 28).
[30] The functional form of the fit to the power spectra was $A_{\text{white}} + A_0\omega_t^4/[(\omega^2-\omega_t^2)^2+\omega^2\omega_t^2/Q^2]$. The fitting parameters are A_{white}, A_0, ω_t, and Q.
[31] Digital Instruments, 112 Robin Hill Road, Santa Barbara, CA 93117.
[32] To ensure that the spheres were aligned with their center of mass as close to the major axis of the cantilever as possible, we measured the horizontal position of the spheres and only used those results in which the off-axis distance was small ($\lesssim 1\ \mu$m).
[33] *Engineering Materials Reference Book*, 2nd ed., edited by M. Bauccio (ASM International, Materials Park, OH, 1994).
[34] S. Ecke, R. Raiteri, E. Bonaccurso, C. Reiner, H. J. Deiseroth, and H. J. Butt, Rev. Sci. Instrum. **72**, 4164 (2001).